Available online at www.sciencedirect.com

ScienceDirect

Procedia Engineering 2 (2010) 1663–1672

Procedia Engineering

www.elsevier.com/locate/procedia

Fatigue 2010

Adjusting the very high cycle fatigue properties of a metastable austenitic stainless steel by means of the martensite content

C. Müller-Bollenhagen*, M. Zimmermann, H.-J. Christ

Institut für Werkstofftechnik, Universität Siegen, D-57068 Siegen, Germany

Received 25 February 2010; revised 9 March 2010; accepted 15 March 2010

Abstract

The effect of deformation induced martensite on the HCF and VHCF properties of austenitic stainless steel sheets in different conditions was studied. In the undeformed condition true VHCF fatigue limit exists even though microplasticity (slip markings) could already be found at a stress amplitude of less than a third of the VHCF fatigue limit and global plastic behavior at less than a half of the VHCF fatigue limit. Fatigue tests with monotonically predeformed specimens in one direction containing different martensite volume fractions showed that the martensite content enhances the HCF and VHCF properties and the fatigue limit remains independent of the cycle number up to 27 vol-%. At 54 vol-% martensite the more brittle behavior and the high notch sensitivity of the martensite phase becomes predominant. This leads to crack initiation at inclusions and a fatigue limit decreasing with the number of cycles in the VHCF regime. By comparing these tests with the behavior of specimens that were monotonically predeformed in two directions, it could be concluded that the VHCF properties are not determined predominantly by the dislocation density, direction of predeformation or amount of predeformation, but by the martensite content, notch sensitivity and the purity of the material. The results lead to the recommendation that automotive stainless steel structures undergoing cyclic loads beyond $2 \cdot 10^6$ cycles should not exceed a deformation-induced martensite content of 27 vol-%.

Keywords: Very High Cycle Fatigue; austenitic stainless steel; deformation-induced martensite; fatigue limit; damage mechanism; microplasticity.

1. Introduction

Due to their beneficial combination of strength and ductility, metastable austenitic stainless steels are widespread for the use in sheet metal forming processes. Plastic deformation during forming can lead to a deformation-induced transformation from the fcc austenite phase to the hcp ε martensite or bcc α' martensite phase [1]. The study presented is concerned with the question, which damage mechanisms are relevant for the HCF (High Cycle Fatigue) and VHCF (Very High Cycle Fatigue) behavior of metastable austenitic stainless steel in the austenitic (undeformed) and austenitic-martensitic (monotonically predeformed) condition. The results are to be used to optimize the HCF and VHCF properties of an automotive part made of austenitic stainless steel sheet by adjusting

* Corresponding author. Tel.: +49-271-740-3419

E-mail address: carsten.mueller-bollenhagen@uni-siegen.de.

1877-7058
doi:10.1016/j.proeng.2010.03.179

the α' martensite content. The automotive part which this study relates to, is the cross bar of a trailer coupling and is formed by a two-step forming process, with the loading directions of the two process steps beeing perpendicular to each other. More details concerning the process can be found in [2]. To characterize the influence of a two-step predeformation on the fatigue properties of austenitic stainless steels, some fatigue specimens were monotonically predeformed in one and some in two directions, both resulting in identical contents of martensite after predeformation.

Martensite can be transformed by a monotonic predeformation as well as under cyclic loading. The rate of transformation strongly depends on the amount of deformation and the temperature of the specimen (Fig. 1). The effect of deformation-induced martensite formation on the VHCF properties is not known so far.

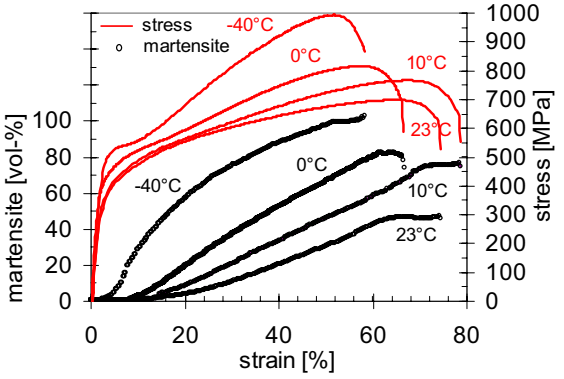

Fig. 1. Martensite formation and stress strain curves at different temperatures (strain rate: 0.5%/s)

Some authors have found that a martensitic phase transformation prior to the fatigue testing is beneficial to the LCF [1] and HCF [3,4] properties of austenitic stainless steel. This effect is mainly attributed to the higher strength of the martensite phase.

In the literature, the VHCF behavior of metallic materials is often classified in type I materials (ductile, without intrinsic defects) and type II materials (materials with intrinsic defects) [5]. Surface roughening caused by local plastic deformation in favorably oriented grains is seen as the predominant damage mechanism in VHCF regime for type I materials (e.g. copper, nickel). Slip markings on the surface can lead to the formation of microcracks [6, 7] that need not necessarily result in crack growth, however. In contrast, type II materials often show local plastic deformation at inclusions that can lead to crack initiation due to debonding of the inclusion-matrix interface or breaking of the non-metallic inclusion. This damage mechanism often leads to the fish-eye fracture surface and was studied by numerous authors for a number of high strength steels, e.g. [8-11]. For both types of materials a decreasing fatigue limit in the VHCF regime can occur [12].

The VHCF behavior of metastable austenitic stainless steel has rarely been investigated yet. Carstensen et al. [13] showed for tubes made of the stable austenitic stainless steel AISI904L that specimens fail beyond 10^8 cycles and the fatigue limit decreases in the VHCF regime. Crack initiation was found only at the outer surface of the tubes without any influence of internal defects. Takahashi and Ogawa [14] found for pre-deformed stable SUS316NG specimens fatigue failure beyond 10^7 cycles. They observed internal crack initiation only in one case without any influence of inclusions. In both papers [13,14] no microstructural reasons for crack initiation were discussed. Chai [15] assumed for an austenitic-martensitic stainless steel, where the martensite was thermally induced, that strain localization in the softer phase or at phase or grain boundaries can lead to a subsurface crack initiation without any influence of inclusions.

The material surveyed in this study is very ductile, in the partially martensitic (predeformed) condition it can exhibit high flow stresses (Fig. 1). Although austenitic stainless steel is known to be of high purity, it can contain numerous types of inclusions [16], which may influence the VHCF behavior.

2. Experimental Details

For all experiments solution annealed metastable austenitic stainless steel sheet (AISI304) with a thickness of 2 mm (before predeformation) and a grain size (mean linear intercept) of 25 µm was used. The chemical composition is given in table 1. For the one-step predeformation a servohydraulic testing machine with a liquid nitrogen-cooled chamber was used. Specimens were strained up to a true plastic strain of $\varphi_x = 0.14$ at starting temperatures of -20°C and -70°C resulting in α' martensite contents of 27 vol-% and 54 vol-%, respectively. The two-step predeformed specimens were deformed at an electromechanical testing machine. First the sheets were strained in one direction, than tensile test specimens were cut out of the sheet perpendicular to the first loading direction (Fig. 2) and strained again. In both cases (one- and two-step deformation) fatigue specimens were cut out of the strained sheets. An overview of he five tested predeformation states, the true strains in x- and y-direction and the related flow stresses can be found in table 2. It can be seen that the flow stresses differ very much depending on the predeformation state. Before fatigue testing, all specimens were mechanically and subsequently electro-chemically polished. For the fatigue experiments two testing systems were used: a resonance pulsation system (Rumul Testronic) operating at ~90 Hz and an ultrasonic test system (BOKU, Vienna) working at a frequency of ~20 kHz. All fatigue experiments were executed in a fully reversed mode under load control. The specimens' geometries used for the two testing systems can be found in Fig. 3. Because of the low thermal conductivity of AISI304 and the relatively high plastic strain amplitudes even in VHCF tests the specimens showed strong self heating and in order to exclude this effect they were actively cooled with compressed air. Temperature was measured at three points T_1, T_2 and T_3 (Fig. 3) with an infrared camera (Flir A-20) or type-K thermocouples. A value for the change in temperature ΔT while fatigue testing was calculated using the equation

$$\Delta T = T_1 - 0.5\,(T_2 + T_3) \qquad (1)$$

It was shown by numerous authors that ΔT correlates directly to the plastic strain amplitude [17, 18], because the plastic work is mainly dissipated as heat. ΔT will be used here instead of the plastic strain amplitude to illustrate cyclic softening and hardening effects in ΔT-N-curves. For some specimens strain was measured by strain gauges as well.

The α' martensite volume fraction was measured by means of a magneto-inductive testing device (Fischer feritscope). X-ray phase analysis showed that the magneto-inductive measurements need to be corrected because the device was originally calibrated to measure the ferrite and not the martensite content. Therefore all martensite fraction values in this study are the feritscope readings corrected with the factor 1.58 to get the true martensite fraction.

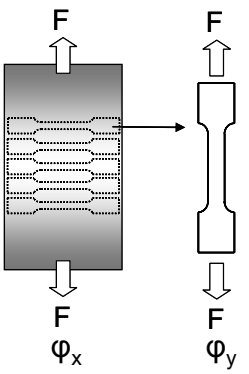

Fig. 2. Two-step deformation of specimens

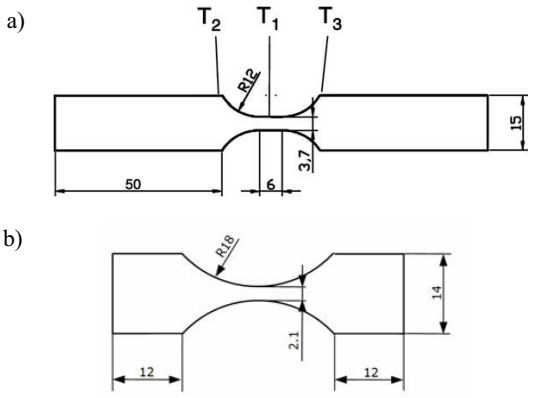

Fig. 3. Specimens' geometries for (a) resonance pulsating system; (b) ultrasonic fatigue system

Table 1. Chemical composition in mass-%

C	*Cu*	*Cr*	*Mo*	*Ni*	*Mn*	*N*
0.024	0.14	18.3	0.04	8.11	1.43	0.067

Table 2. True strains in x- and y-direction (φ_x φ_y) and flow stresses of the specimens in different testing conditions

	martensite	φ_x	φ_y	flow stress [MPa]
not predeformed	0 vol-%	0	-	284
one-step predeformed	27 vol-%	0.14	-	652
	54 vol-%	0.14	-	752
two-step predeformed	27 vol-%	0.27*	0.15	996
	54 vol-%	0.27*	0.22	1063

* φ_x in the two-step deformed condition is higher than in the one-step case to reach the same martensite fraction without cooling, cp. subsection 3.2.2.

3. Results

3.1. Fatigue behavior in the fully austenitic condition

In the fully austenitic condition, the metastable austenitic stainless steel studied exhibits a constant fatigue limit in the VHCF regime of 250 MPa (Fig. 4). Even below this fatigue limit, at 240 MPa, the specimens show strong softening at the beginning of the test (Fig. 5 – increasing ΔT and strain amplitude up to $6{\cdot}10^4$ cycles), and hardening afterwards (Fig. 5 – decreasing ΔT and strain amplitude beyond $6{\cdot}10^4$ cycles). No specimen in Fig. 4 showed evidence of subsurface crack initiation. No specimen failed beyond 10^6 cycles, even though remarkable surface roughening (slip markings, extrusions) and martensite lamellae could be observed on the surface of run-out specimens, see ref. [19] for details. The stress-strain hysteresises in Fig. 6 prove that the assumption the global cyclic behavior in the VHCF regime being solely elastic is not met for the material studied. Even though the plastic work (e.g. the area of hysteresis) at 10^7 cycles is a lot smaller than at $6{\cdot}10^4$, the deformation behavior of the material is not purely elastic.

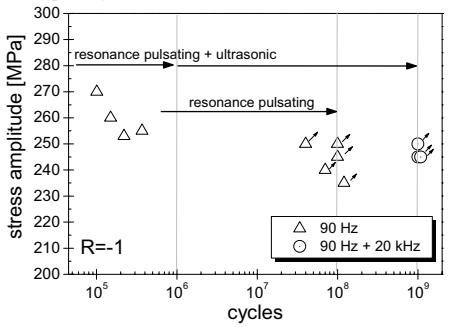

Fig. 4. S-N curve of electro-chemically polished specimens fatigued by resonance pulsation and ultrasonic testing (arrows indicate run-out specimens).

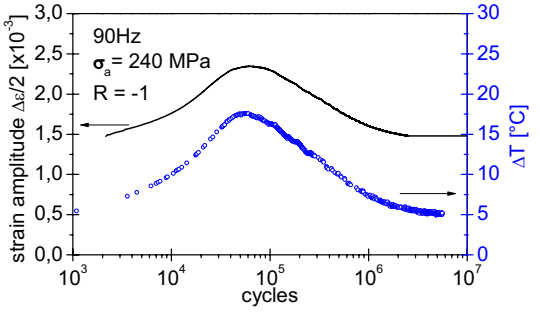

Fig. 5. Comparison of ε_a-N and ΔT-N at 240 MPa.

In order to determine at which load amplitude irreversible plastic deformation starts, a load-increase test at 20kHz was executed with the ultrasonic test system. Due to the very high frequency, the time to conduct the dissipated heat energy is short. Therefore even a small amount of local plastic deformation per load cycle can lead to a measurable increase in the temperature of the specimen. Consequently, to identify the stress amplitude where local plastic deformation starts, the increase in temperature was measured by means of a thermocouple and the strain amplitude by means of a strain gauge. For this test no active cooling was used. Stress values were calculated from the strain amplitude measurements using Hook's law and a Young's Modulus of 190 GPa. Starting from 54 MPa, the stress amplitude was raised every 10^6 cycles for 16 MPa. At the end of every load step the originally electro-chemically polished surface of the specimen was analyzed by optical microscopy. Fig. 7 shows the increase in the temperature ΔT for every load step. In the first two load steps the increase in temperature is negligible. Here the increase in

temperature is below 1°C, what might be due to internal friction processes [20,21]. Then, at a load of 86 MPa, the temperature starts to increase significantly up to a ΔT of 6°C. This increase in temperature represents the beginning of (local) plastic deformation at this stress amplitude. Since the global elastic limit is remarkably higher (0.2% proof stress is 284 MPa), plastic deformation was not expected at this stress amplitude that is not even one third of the proof stress and about one third of the 10^9-fatigue limit.

Optical microscopy observations affirm the beginning of plastic deformation at 86 MPa. In Fig. 8a)-f) micrographs of the surface of the specimen after the first four load steps are shown. Before cycling and after the first load step no changes are observable on the surface (Fig. 8a+b). After the 70 MPa load step one slip markings can be observed (Fig. 9c). Then, it can clearly be seen that at 86 MPa many slip markings were formed on the surface (Fig. 8d), some are indicated by arrows. To visualize the grain boundaries, an SEM image was combined with an optical microscopy picture after the 102 MPa load step (Fig. 8e). Slip markings are only visible in some grains, with the slip markings covering the full length of the grain. By comparing the grains with slip markings with Schmid factors calculated from EBSD-data (Fig. 8f), it becomes clear that not only grains with maximum Schmid factor show slip band formation. Magneto-inductive measurements and microscopic observations give evidence that no formation of martensite in the load-increase test has occured.

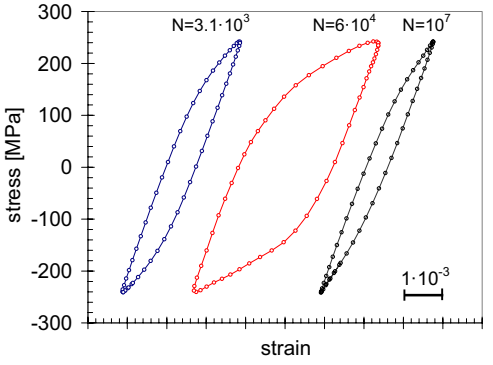

Fig. 6. Stress strain hysteresis at different number of cycles, Δσ/2=240 MPa, f≈90Hz

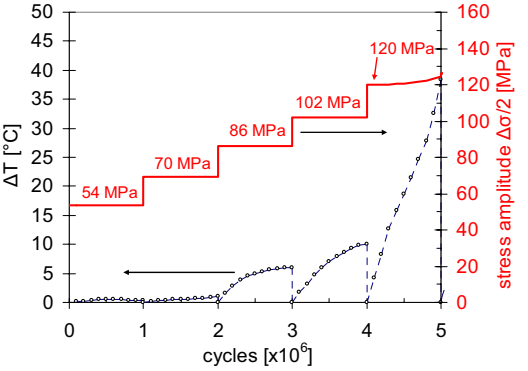

Fig. 7. Temperature increase in a load-increase test at 20 kHz

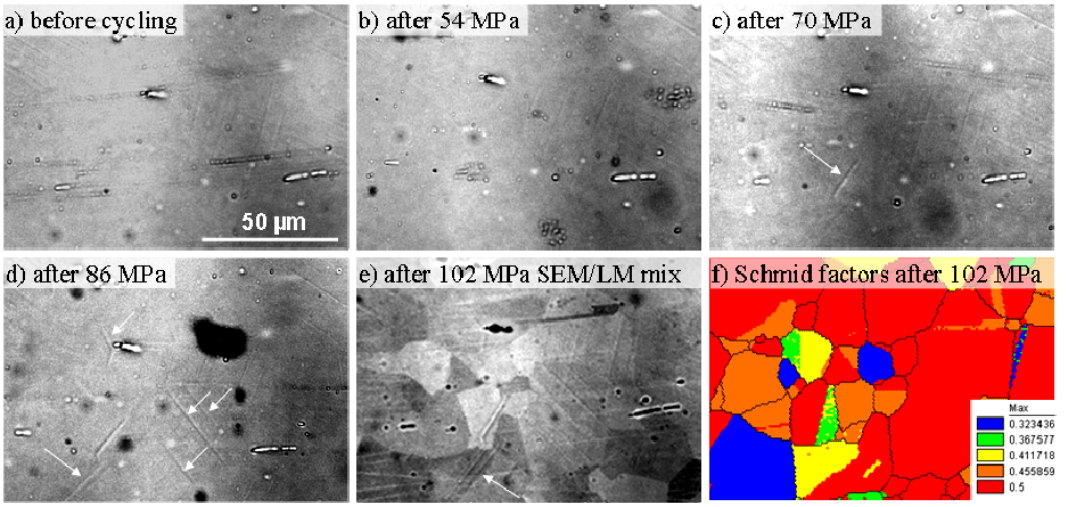

Fig. 8. Micrographs of a specimen's surface after different load steps; a)-d) are perceived by means of optical microscope, e) is a combination of an SEM and an optical microscope picture; f) shows the Schmid factors derived from EBSD data.

3.2. Fatigue behavior in the predeformed condition

In order to develop a quantitative relationship between the volume fraction of martensite and the VHCF behavior specimens were monotonically prestrained in two different ways, as described in section 2. The subsequent fatigue results will be described in the two following subsections.

3.2.1. Fatigue behavior in the one-step predeformed condition

Specimens with the same amount of monotonic plastic deformation (φ_x=0.14) but different volume fractions of martensite (because of different predeformation temperatures) were fatigued in order to find a quantitative relationship between martensite fraction and VHCF lifetime. Two kinds of specimens were tested: specimens with an α' martensite content of 27±2 vol-% and specimens with an α' martensite content of 54±2 vol-%. The results are given in Fig. 9. Open symbols indicate samples fatigued with the a resonance pulsation system up to 10^8 cycles. Crossed symbols represent samples fatigued firstly with the resonance pulsation system up to cyclic saturation ($2 \cdot 10^6$ cycles) and subsequently cycled up to 10^9 cycles in the ultrasonic test system. Fig. 9 shows that for the 27 vol-% martensite specimens there is a constant fatigue limit (475 MPa) in the VHCF regime that is equal to that in the HCF regime. In this condition no specimen failed beyond $2 \cdot 10^6$ cycles. In the 54 vol-% martensite condition the VHCF behavior is different: There are failures up to $6.84 \cdot 10^8$ cycles and the fatigue limit is decreasing in the VHCF regime. All specimens that failed above $3 \cdot 10^6$ cycles failed because of internal crack initiation at an inclusion. EDX analysis of the inclusions showed high contents of Cr, Ti, Al and O, indicating that the inclusions are oxidic particles originating from impurities in the melt. The inclusions geometry appears to be mostly circular or oval with an average area of 150 µm². The subsurface crack initiation leads to a typical appearance of the fracture surface mainly observed for type II materials, the fisheye fracture, as can be seen in Fig. 10. All specimens with subsurface crack initiation showed this typical fractographic feature.

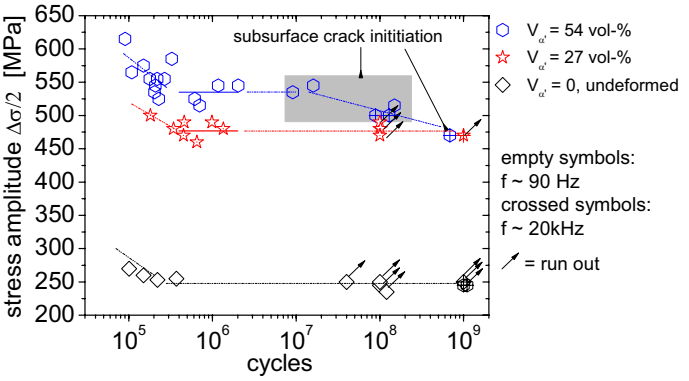

Fig. 9. S-N curves for one-step deformed specimens with different martensite contents.

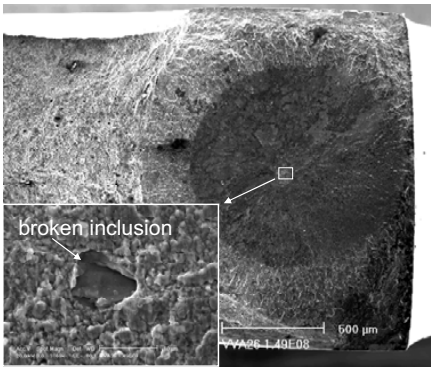

Fig. 10. Subsurface crack initiation for a specimen with 54 vol-% martensite that failed at $N=1.49 \cdot 10^8$.

3.2.2. Fatigue behavior in the two-step predeformed condition

Two-step predeformed specimens with the same volume percent of martensite as the one-step predeformed specimens (27 and 54 vol-%) were fatigued. No cooling was applied here during predeformation. Therefore, to get the same amount of martensite as in the (cooled) one-step tests, higher amounts of deformation were necessary that resulted in a distinctly higher flow stress (e.g. 1063 MPa vs. 752 MPa for 54 vol-% martensite, table 2). The values for the true strains in the two directions are given in table 2. Comparing the fatigue properties of the material in both conditions (one and two-step deformed) aims to answer the question, which microstructural properties are vital for the VHCF properties: dislocation-induced hardening, martensite content or notch sensitivity (regarding inclusions or surface defects). Fig. 11 shows, that the VHCF fatigue limit of the two-step predeformed specimens has the same gradient as the one-step one for 54 vol-%. Interestingly, although the two-step specimens that failed above $2 \cdot 10^6$

cycles, also failed because of cracks starting at inclusions, crack initiation shifted from the inside of the specimens to the surface or near-surface region (Fig. 12). The two-step deformed specimens with 27 vol-% martensite showed behavior similar to the one-step deformed specimens with 27 vol-% martensite. Again, at 27 vol-% the fatigue limit is constant in the VHCF regime and there is no specimen failure above 10^6 cycles.

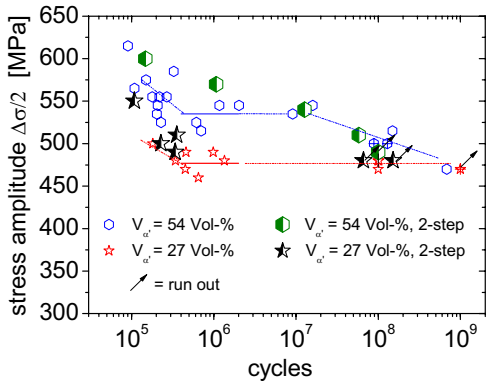

Fig. 11. S-N curves for two-step deformed specimens with different martensite contents.

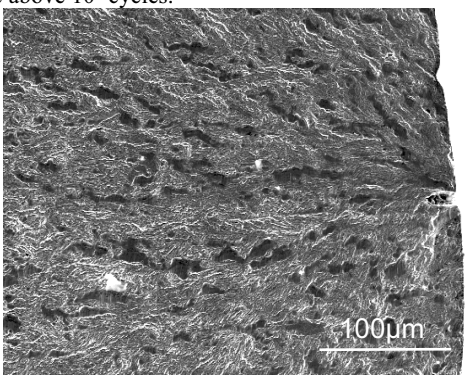

Fig. 12. Crack initiation at a near-surface inclusion at a two-step deformed specimen (N_B=1,27·10^7).

4. Discussion

In the undeformed condition, the tested material shows plastic deformation (connected with a pronounced temperature increase) during cyclic loading well below the VHCF fatigue limit (Fig. 6-8). Even at 86 MPa strain localization in slip bands can be observed microscopically. This supports the assumption, that a significant rise in the specimen temperature is always connected to microplasticity. Internal friction, the other conceivable reason for an increase in temperature, is far less pronounced (~1°C for 70 MPa) and even in this load step evidence of microplasticity was found in one grain (Fig. 7c).

At the end of the last load step (as shown in Fig. 7) the beginning of cyclic softening can be observed, indicated by an increasing value for the stress amplitude (the test is displacement controlled). The increase in temperature at 86 and 102 MPa converges to a horizontal asymptote and is therefore not due to cyclic softening. At the last load step, the increase in stress amplitude was 18 MPa instead of 16 MPa, because due to cyclic softening there is no linear relationship between displacement and stress amplitude anymore. Hence, above 102 MPa not only global plastic deformation, but also transient behavior must be considered regarding the VHCF behavior of austenitic stainless steel. Interestingly, the plastic deformation, that has at least at 240 MPa (Fig. 4) a strong global character, does not lead to a failure at very high number of cycles. It is most likely that this is due to the cyclic hardening that reduces the plastic strain amplitude to a level that is smaller than the critical strain amplitude for crack growth. According to TEM observations by Nebel [22] and in situ martensite measurements by Nikitin and Besel [23] the cyclic hardening is caused by the formation of martensite and an increase in the dislocation density, what is consistent with the experiments in this study, where martensite volume fractions of 3% to 5% were found in specimens cycled below the fatigue limit. SEM examination of cycled specimens proved that martensite needles are formed in grains with strong slip band formation, thus indicating that hardening due to martensite formation takes place in grains with high plastic activity on active slip planes. Some more details concerning these observations can be found in [19,24]. Without these hardening mechanisms, the VHCF fatigue limit would most likely be less than half of the actual value. The finding that the local formation of martensite is a major reason for the infinite fatigue life is supported by the fact that in a stable austenitic stainless steel a decreasing fatigue limit was found in [13]. The strong affinity of this material to local and global plastic activity under extremely small loads (Fig. 7+8) and the significant strain amplitudes in the range of the VHCF fatigue limit (Fig. 6) must be taken into consideration, if this material is used for high-precision or safety-relevant parts subjected to cyclic loads. Besides, it has to be considered

that the positive effect of martensite–assisted cyclic hardening decreases with increasing temperature, if parts are cyclically loaded at elevated temperatures. The VHCF fatigue limit then might be well below the values in this study.

In the one-step predeformed condition, the HCF properties can clearly be improved by increasing the martensite content from 27 to 54 vol-%. However, the VHCF fatigue limit starts to decrease at the higher martensite fraction because of an increased affinity to subsurface crack initiation at inclusions that can be seen as micro-notches. An increasing notch sensitivity with increasing martensite contents could already be observed by the authors in HCF tests with micro-notched specimens [19]. A likely reason for the increasing notch sensitivity is illustrated in Fig. 13. It shows the phase distribution of austenite and martensite on the surface of two specimens with 25 and 54 vol-% of martensite. The martensite is colored black.

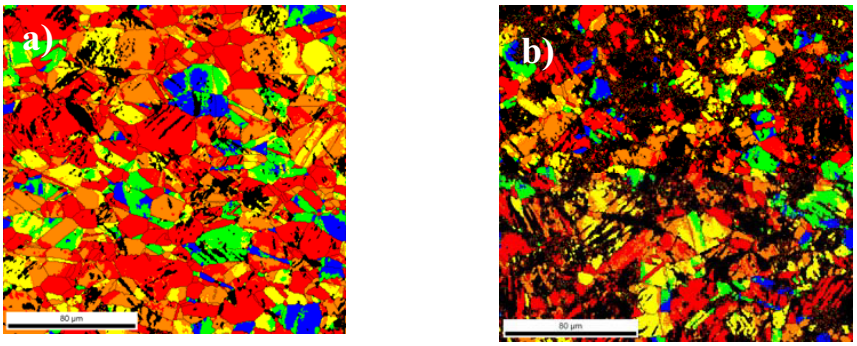

Fig. 13. EBSD images of the surface of specimens with martensite contents of a) 25.3 Vol-% and b) 54 Vol-%. Martensite appears black.

In Fig. 13a, it can be seen that isolated martensite needles appear in austenitic grains. At the higher martensite content (Fig. 13b), some austenite grains are completely transformed into martensite and the martensitic areas are mostly connected to each other so that they build a continuous network. Considering the microstructure of the bulk material this effect is even more significant than can be observed at the surface, because the martensite content increases with increasing distance from the surface. By means of in situ X-ray stress measurements in tensile tests, Talonen [25] found that above 30 vol-% of martensite the macroscopic stress is increasingly influenced by the martensite phase, whereas below 30 vol-% it is mainly equal to the austenite stress. This is consistent with the results in this study. The higher strength and brittleness of the martensite phase and therefore higher notch sensitivity becomes predominant at martensite contents higher than 30 vol-%. A reason for the crack initiation at inclusions only at high martensite contents may be concluded from Fig. 13: at 25 vol-% the typically needle shaped martensitic areas are mostly smaller than the inclusions that have an average diameter of about 14 µm (calculated from their average area under the assumption of a globular shape). As a consequence, no (or at least very few) inclusions will be surrounded only by martensite. Hence, the high local stresses at the inclusion-matrix interface can be compensated by slip activity in the softer austenite phase. If nevertheless a crack is initiated, phase transformation at the crack tip may cause compressive stresses due to the higher volume of the martensite phase [1,24,26] and hinder crack growth. Looking at the microstructure in Fig. 13b, martensite network areas are much larger than the average inclusion size, implying that at least some inclusions will most likely be completely encircled by the martensite phase. The combination of a higher notch sensitivity of the martensite phase and the lack of compensatory slip activities outbalancing the incompatability stresses between inclusion and matrix can lead to crack initiation in the hard martensite phase. Then no phase transformation at the crack tip can take place and hinder crack growth.

The fatigue tests with the two-step predeformed specimens (Fig. 11) showed that not the strength or the dislocation density of the austenite phase determines the VHCF properties, but the volume fraction of martensite. Although the flow stress is more then 300 MPa higher for the two-step deformed specimens (table 2), the VHCF strength is similar to that of the one-step deformed specimens with the same martensite fraction. In both 27 vol-% martensite conditions there is no failure of specimen above $2 \cdot 10^6$, despite the fact, that the strengths (and therefore

the dislocation densities) are very different. This supports the assumption that the combination of martensite content and inclusion size plays a decisive role for the VHCF behavior and not the yield stress, dislocation density or direction of predeformation.

Regarding the question, if the metastable austenitic stainless steel studied can be classified as type I or type II material (cp. section 1), one must conclude that this material shows typical characteristics for both types, depending predominantly on the volume fraction of martensite. In the fully austenitic condition, austenitic stainless steel shows clear type I behavior with inhomogeneous surface roughening due to local plastic deformation (Fig. 7) and local surface roughening due to martensite formation [19]. But as a consequence of the strong softening and hardening mechanisms, only non-propagating microcracks are initiated, so no specimen failure takes place in the VHCF regime. The inclusions have no influence on the damage mechanism in this condition. In the 27 vol-% martensite condition still surface roughening takes place and there is no subsurface crack initiation at inclusions. At 54 vol-% the material shows typical type II damage behavior, with cracks initiating around subsurface inclusions, showing fisheye-type fracture surfaces and a therefore decreasing fatigue limit.

These results show that the VHCF damage mechanisms for the same material can be very different for different conditions of deformation and cannot be derived from the classical fatigue behavior in the HCF regime, what should be considered while planning an optimal sheet metal forming process. Hence, based on the findings of the study presented, automotive stainless steel structures that undergo cyclic loads beyond $2 \cdot 10^6$ cycles should not exceed a martensite content of 27 vol-%.

5. Conclusions

- Local plastic deformation starts at very small load amplitudes (about one third of the VHCF fatigue limit) in metastable austenitic stainless steel and can be identified due to slip markings at the surface. The strong self-heating of austenitic stainless steel is mostly due to microplasticity and only to a small amount induced by internal friction.
- In the fully austenitic condition a true VHCF fatigue limit exists, even though remarkable plastic strain amplitudes occur. The constant fatigue limit is caused by a martensite-assisted cyclic hardening process.
- The martensite content enhances the HCF properties and the VHCF fatigue limit remains independent of the cycle number in the VHCF regime up to 27 vol-% martensite.
- At 54 vol-% martensite the more brittle behavior and higher notch sensitivity of the martensite phase becomes predominant and leads to crack initiation at inclusions in the VHCF regime. This effect is attributed to the fact that the dimensions of the martensitic domains exceed the dimensions of the average inclusion size by forming martensitic networks thus preventing a compensation of local incompatability stresses between inclusions and matrix.
- The VHCF properties are not determined predominantly by the dislocation density, direction of predeformation or amount of predeformation, but by the martensite content, notch sensitivity and the purity of the material.
- Automotive stainless steel structures that undergo cyclic loads beyond $2 \cdot 10^6$ cycles should not exceed a deformation-induced martensite content of 27 vol-%.

Acknowledgements

The authors gratefully acknowledge the financial support of this study by Deutsche Forschungsgemeinschaft (DFG).

References

[1] Maier HJ, Donth B, Bayerlein M, Mughrabi H, Maier B, Kesten M. Optimierte Festigkeitssteigerung eines metastabilen austenitischen Stahles durch verformungsinduzierte Martensitumwandlung bei tiefen Temperaturen. *Z Metallkd* 1993;**84**(12):820-26.

[2] Müller-Bollenhagen C, Zimmermann M, Christ H-J, Schröder X, Engel B, Große-Wöhrmann A, Suttmeier F-T. Modelling and closed-loop control of complex tube forming based on an optimized application of martensite formation in austenitic stainless steels. *Steel Res Int* 2008;**79**(10):745-52.

[3] Myeon TH, Yamabayashi Y, Shimojo M, Higo Y. A new life extension method for high cycle fatigue using micro martensitic transformation in austenitic stainless steel. *Int J Fatigue* 1997;**19**(93):69-73.

[4] Topic M, Tait RB, Allen C. The fatigue behaviour of metastable (AISI-304) austenitic stainless steel wires. *Int J Fatigue* 2007;**29**(4):656–65.

[5]Mughrabi H. Specific features and mechanisms of fatigue in the ultrahigh-cycle regime. *Int J Fatigue* 2006;**28**(11):1501-8.

[6] Chan KS. Roles of microstructure in fatigue crack initiation. *Int J Fatigue* 2009; In Press doi:10.1016/j.ijfatigue.2009.10.005.

[7] Knobbe H, Köster P, Krupp U, Christ H-J, Fritzen K-P. Microstructural aspects of duplex steel during high cycle and very high cycle fatigue. Proceedings of the 15th International Conference on the Strength of Materials, Dresden (2009) to be published in: *Journal of physics: conference series.*

[8] Murakami Y, Yokoyama, NN, Nagata, J. Mechanisms of fatigue failure in ultralong life regime. *Fatigue Fract Engng Mater Struct* 2002;**25**:735-46.

[9] Liu YB, Yanga ZG, Li YD, Chena SM, Li SX, Hui WJ, Weng YQ. Dependence of fatigue strength on inclusion size for high-strength steels in very high cycle fatigue regime. *Mater Sci Eng A* 2009;**517**:180-84.

[10] Sakai T. Review and prospects for current studies on very high cycle fatigue in metallic materials for machine structural use, *J. Solid Mech. and Mat. Eng*. 2009;**3**(3):425-39.

[11] Bathias C. Influence of the metallurgical instability on the gigacycle fatigue regime. *Int J Fatigue* 2010;**32**(3):535-40.

[12] Berger C, Pyttel B, Schwerdt D. Beyond HCF - Is there a fatigue limit?. *Materialwiss Werkstofftech* 2008;**39**(10):769-76.

[13] Carstensen JV, Mayer H, Brondsted P. Very high cycle regime fatigue of thin walled tubes made from austenitic stainless steel, *Fatigue Fract Eng Mater Struct* 2002;**25**(8-9):837-44.

[14] Takahashi K, Ogawa T. Evaluation of giga-cycle fatigue properties of austenitic stainless steels using ultrasonic fatigue test. *Solid Mech and Mat Eng* 2008;**2**(3):366-73.

[15] Chai G. The formation of subsurface non-defect fatigue crack origins. *Int J Fatigue* 2006;**28**(11):1533–1539.

[16] Lo KH, Shek CH, Lai JKL. Recent developments in stainless steels, *Mater Sci Eng: R Reports* 2009;**65**(4-6):39-104.

[17] Smaga M, Walther F, Eifler D. Investigation and modelling of the plasticity-induced martensite formation in metastable austenites. *Int J Mat Res* 2006;**97**(12):1648-55.

[18] Wagner V, Ebel-Wolf B, Walther F, Eifler D. Very high cycle fatigue of railway wheel steels. *Proc. of the 4. Int. Conf. on Very High Cycle Fatigue*, Allison JE, Jones JW, Larsen JM, Ritchie RO, editors. TMS Publications, 2007, p. 137-42.

[19] Müller-Bollenhagen C, Zimmermann M, Christ H-J. Very high cycle fatigue behaviour of austenitic stainless steel and the effect of strain-induced martensite, *Int J Fatigue* 2010;**32**:936-42.

[20] Maquin F, Pierron F. Heat dissipation measurements in low stress cyclic loading of metallic materials: From internal friction to micro-plasticity. *Mech Mater* 2009;**41**(8):928-42.

[21] Cugy P, Galtier A. Microplasticity and temperature increase in low carbon steel. *Proc. of the 8th Int. Fatigue Congress*, vol. 1, Blom AF, editor. EMAS; 2007, p. 549-56.

[22] Nebel T. Verformungsverhalten und Mikrostruktur zyklisch beanspruchter metastabiler austenitischer Stähle. doctorate thesis, Universität Kaiserslautern, Germany, 2002.

[23] Nikitin I, Besel M. Effect of low-frequency on fatigue behaviour of austenitic steel AISI304 at room temperature and 25 °C. *Int J Fatigue* 2008;**30**(10-11):2044–49.

[24] Christ H-J, Krupp U, Müller-Bollenhagen C, Roth I, Zimmermann M. Effect of deformation-induced martensite on the fatigue behavior of metastable austenitic stainless steels, *Proceedings of the 12th international conference on fracture*, Ottawa, Kanada, 2009, CD-ROM.

[25] Talonen J. Effect of strain-induced α'-martensite transformation on mechanical properties of metastable austenitic stainless steels, Doctorate thesis, Helsinki University of Technology, Finnland, 2007.

[26] Suresh S. Fatigue of Materials, 2nd edition, Cambridge:Cambridge University Press; 2006.